Engineering Structures 88 (2015) 225–240

Contents lists available at ScienceDirect

Engineering Structures

journal homepage: www.elsevier.com/locate/engstruct

Effects of truss behaviour on critical temperatures of welded steel tubular truss members exposed to uniform fire

E. Ozyurt, Y.C. Wang *

School of Mechanical, Aerospace and Civil Engineering, University of Manchester, UK

ARTICLE INFO

Article history:
Received 8 March 2014
Revised 10 October 2014
Accepted 19 January 2015

Keywords:
Circular Hollow Section (CHS)
Finite element (FE)
Critical temperature
Truss member limiting temperatures

ABSTRACT

This paper presents the results of a numerical investigation into the behaviour of welded steel tubular truss at elevated temperatures. The purpose is to assess whether the current method of calculating truss member limiting temperature, based on considering each individual truss member and using the member force from ambient temperature analysis, is suitable. Finite Element (FE) simulations were carried out for Circular Hollow Section (CHS) trusses using the commercial Finite Element software ABAQUS v6.10-1. The FE simulation model had been validated against available fire test results on trusses. The simulated trusses were subjected to constant mechanical loads and then increasing temperatures until failure. The elevated temperature stress–strain curves were based on Eurocode EN-1993-1-2. Initial geometrical imperfections were included, based on the lowest buckling mode from eigenvalue analysis.

The numerical parametric study examined the effects of truss type, joint type, truss span-to-depth ratio, critical member slenderness, applied load ratio, number of brace members, initial imperfection and thermal elongation on critical temperatures of the critical truss members.

These critical temperatures were then compared with the member-based critical temperatures, which were numerically calculated using ABAQUS but using the member forces obtained from ambient temperature structural analysis as would be the case in the current design method.

The results of the numerical parametric study indicate that due to truss undergoing large displacements at elevated temperatures, some truss members (compression brace members near the truss centre) experience large increases in member forces. Therefore, when calculating the member critical temperatures, it would not be safe to use the member forces from the ambient temperature structural analysis. Using the ambient temperature member force may overestimate the truss member critical temperature (based on truss analysis) by 100 °C.

Finally, this paper proposes and validates an analytical method to take into consideration the additional compression force due to large truss displacement. This is based on assuming a maximum truss displacement of span over 30.

© 2015 Elsevier Ltd. All rights reserved.

1. Introduction

Hollow structural sections of all types are widely used in truss construction due to their attractive appearance, light weight and structural advantages. They are commonly used in onshore and offshore structures e.g. bridges, towers, stadiums, airports, railway stations, offshore platforms etc. For these structures, fire presents one of the most severe design conditions, because the mechanical properties of the steel degrade as the temperature increases.

For truss design, both the members and the joints should be checked. Truss member design at ambient temperature is relatively easy, involving mainly design checks for tension and compression resistance after performing static analysis to obtain the member forces. There is abundant amount of literature on the behaviour and strength and of truss joints at ambient temperature. Indeed, the CIDECT design guide [3] and Eurocode EN 1993-1-8 [4] present design equations to calculate the ambient temperature static strength of practically all tubular truss joints. In comparison, there are only a few research studies on welded joints at elevated temperatures. Among them, Nguyen et al. [5,6] carried out both experimental and numerical analysis on the behaviour of five full scale Circular Hollow Section (CHS) T-joints subjected to axial compression in the brace member at different temperatures. Meng et al. [7] and Liu et al. [8] presented a limited amount of experimental and parametric data of the structural behaviour of

* Corresponding author.
E-mail address: yong.wang@manchester.ac.uk (Y.C. Wang).

http://dx.doi.org/10.1016/j.engstruct.2015.01.032
0141-0296/© 2015 Elsevier Ltd. All rights reserved.

steel planar tubular trusses subjected to fire. Chen and Zhang [9] tested and numerically modelled a steel roof truss without fire-proof coating under localised pool fire condition to obtain information on temperature distributions and displacements. However, no information was provided on failure mode or failure temperatures of the truss. Yu et al. [10] examined the mechanical behaviour of a steel T-joint under fire after impact loading. They observed increased failure temperature in the subsequent fire test compared to the fire test without impact. They attributed this increase to increased steel mechanical properties after high strain impact load. Jin et al. [11] experimentally investigated the parameters that affect post-fire behaviour of tubular T-joints. Based on their test results, they found that the load ratio in the brace member had no effect on the residual bearing capacity of the T-joint during both heating and cooling. Cheng et al. [12] observed that the critical mode of joint failure was plastification of the chord face for CHS T-joints at elevated temperatures with the brace member in compression. He et al. [13] carried out experimental tests to investigate fire resistance and failure mode of two full scale CHS K-joints under brace axial loading at brace ends. It was noted that the final failure mode of the two tests was due to local plastic yielding on the chord surface at brace-to-chord intersection area. The authors [14] recently developed and validated a design method for calculating the static strength of welded truss joints at elevated temperatures.

Under fire condition, the current method for truss member design involves calculating the member force using static analysis at ambient temperature and then finding the critical temperature, defined as the maximum temperature at which the member can resist the applied load, using the ambient temperature member force. The member force – critical temperature relationship can be evaluated using design methods such as those in BS 5950 Part 8 [15] and EN 1993-1-2 [2]. However, the member force obtained from truss static analysis at ambient temperature may not be correct at elevated temperatures due to large deformations of the truss. The review in the previous section indicates that there has been little study to investigate how truss member forces change at elevated temperatures and how such changes affect the member critical temperatures. These are the topics of the present paper.

The specific scope of this paper is to investigate whether the member-based fire resistance design approach is safe, and if not, to develop a modified member-based method to take into consideration truss behaviour.

2. Validation of finite element model

The results of this paper are based on numerical simulations using the general finite element package ABAQUS/Standard v6.10-1 [1]. For validation, the fire tests of Edwards [16] and Liu et al. [8] were simulated and compared with the test results.

Figs. 1 and 2 show the tested trusses. Failure modes and displacement-temperature curves were compared.

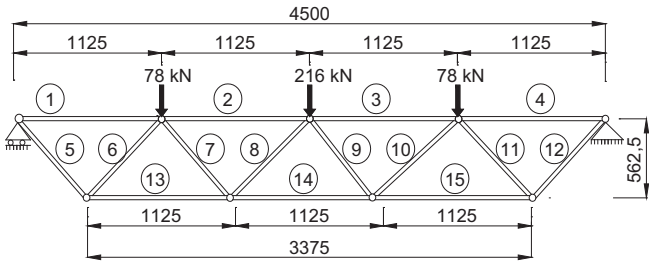

Fig. 1. Test Girder B of Edwards [16] (dimensions in mm).

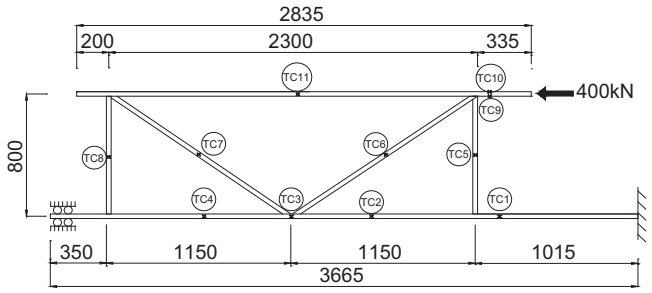

Fig. 2. Test specimen SP1 of Liu et al. [8] (dimensions in mm).

2.1. Material properties

Table 1 summarises the member sizes and material grades. For both tests, the ambient temperature mechanical properties were based on their coupon results. Extensive temperature measurements of the truss members were made in both tests and the recorded temperatures were used in the numerical analysis.

The elevated temperature engineering stress–strain curves were based on Eurocode EN-1993-1-2 as shown in Fig. 3 [2]. In the ABAQUS simulation model, the engineering stress–strain curve was converted into a true stress and logarithmic strain curve to consider nonlinear effects of large displacements by using the following equations [17]:

$$\varepsilon_T = \ln(1+\varepsilon) \tag{1}$$

$$\sigma_T = \sigma.(1+\varepsilon) \tag{2}$$

where ε_T, is the true strain, ε, is the engineering strain, σ_T, is the true stress and σ, is the engineering stress.

2.2. Finite element type and initial imperfection

For the chord and brace members, ABAQUS element types S4R (4 noded shell element) or B21 (2 noded line element) may be used. In the case of modelling using shell elements, quadratic wedge solid elements (C3D15) instead of shell elements were used for the weld to allow accurate meshing of the weld geometry [18]. At the weld-tubular section interface, the brace and chord members were tied with the weld elements using the ABAQUS "tie" function with surface to surface contact. The brace and chord members were chosen as the master surface and the weld elements the slave surface. Owing to symmetry in loading and geometry, to reduce computational time, only half of the truss was modelled when using shell elements, with the boundary conditions for symmetry being applied to the nodes in the various planes of symmetry as shown in Fig. 4.

Eigenvalue buckling analysis was performed on the numerical models in order to define the possible buckling modes for compressed members in the trusses. Lanczos was chosen as eigensolver together with the request five buckling modes [1]. Initial imperfections were included, based on the lowest buckling mode from eigenvalue analysis. The maximum initial imperfection was according to EN 1993-1-1 [19].

2.3. Comparison with test results

2.3.1. Test SP1 of Liu et al. [8]

Fig. 5 shows the recorded test temperatures (see Fig. 2 for locations of the thermocouples). These temperature curves were used in the numerical simulation.

The SP1 truss failed due to buckling of the diagonal brace member in compression. Fig. 6 compares the observed failure mode of

Table 1
Dimensions and ambient temperature mechanical properties of the test trusses.

Member type	Dimensions (mm)	Steel grade	Young's modulus (GPa)	Yield stress (MPa)	Tensile stress (MPa)
Girder B [16]	SHS				
Inner bracings (Member 7, 8, 9 and 10)	60 × 60 × 4.0	43C (S275)	190	384.92	487.38
Outer bracings (Member 5,6, 11 and 12)	60 × 60 × 8.0	43C (S275)	190	279.93	436.63
Top chord (Member 1, 2, 3 and 4)	100 × 100 × 10.0	50C (S355)	210	397.16	574.49
Bottom chord (Member 13, 14 and 15)	100 × 100 × 10.0	50C (S355)	210	397.16	574.49
SP1 [8]	CHS				
Brace	102 × 5	Q345B	202	376	559
Top chord	180 × 8	Q345B	193	368	553
Bottom chord	219 × 8	Q345B	196	381	565

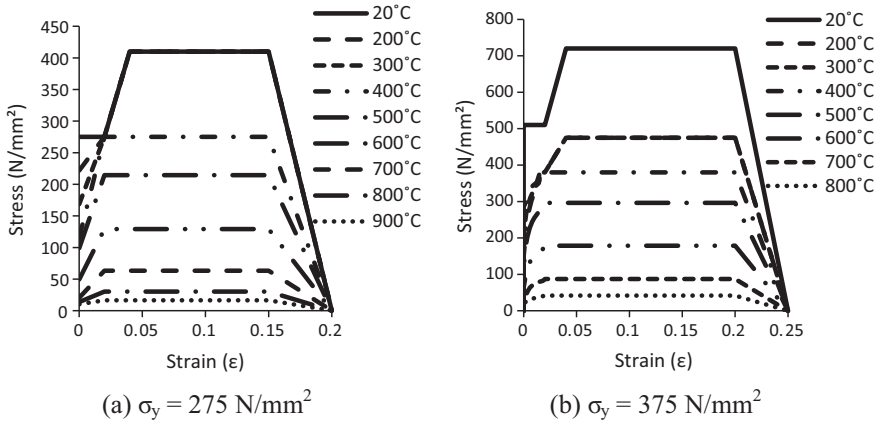

Fig. 3. Engineering stress–strain relationships of steel at elevated temperatures (according to EN 1993-1-2 [2]).

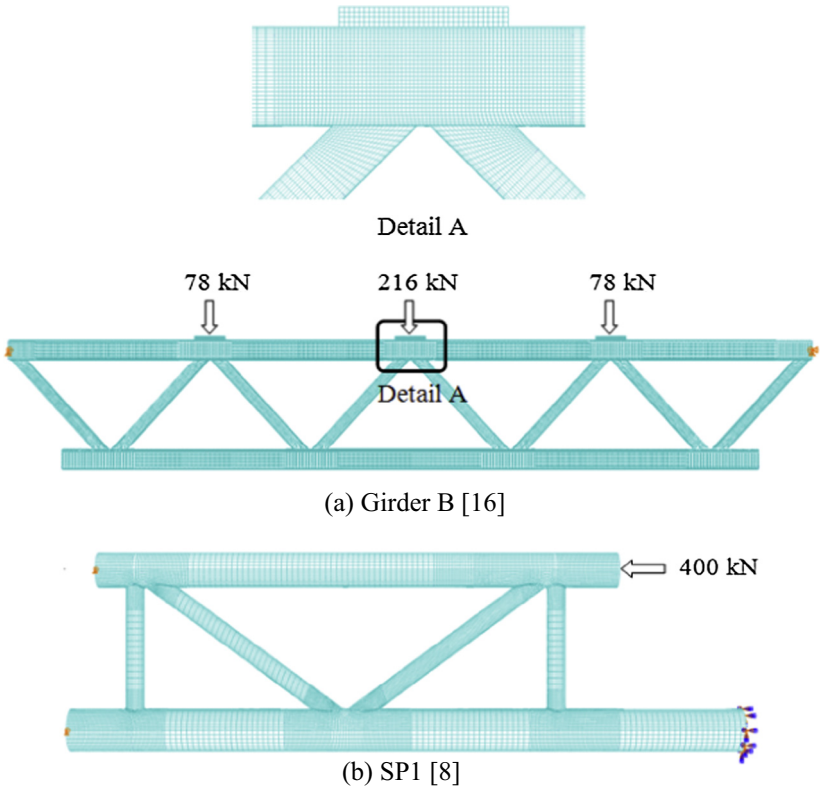

Fig. 4. Finite element models of the test trusses for validation study.

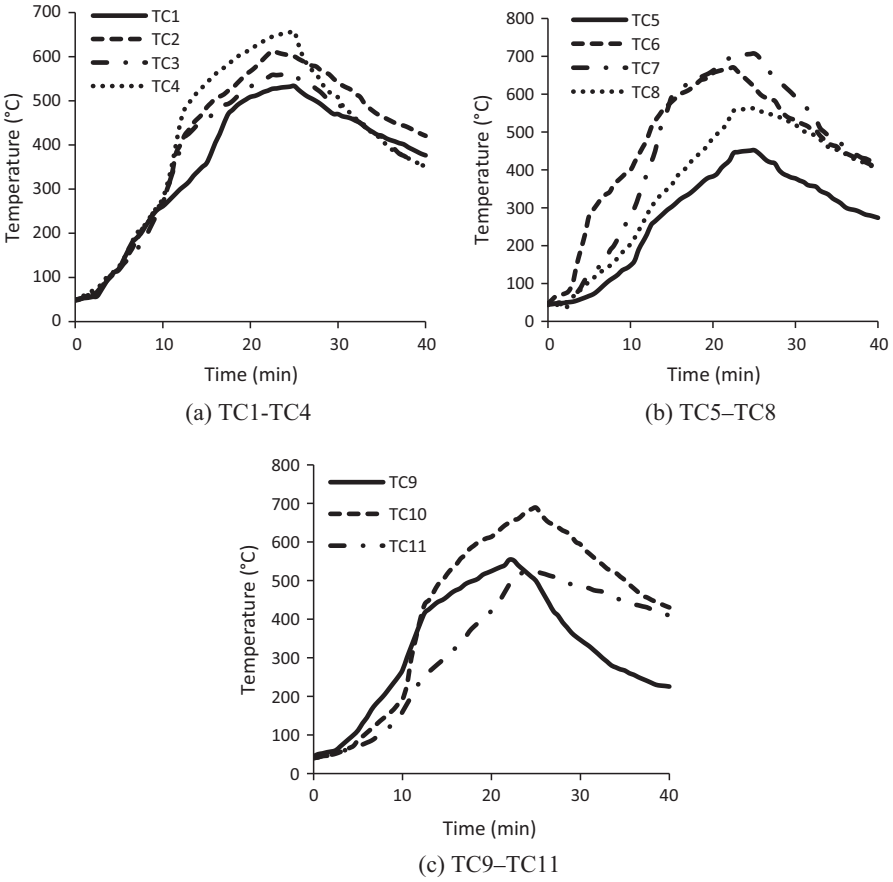

Fig. 5. Recorded temperature–time curves of thermocouples TC1 – TC11 for test SP1 [8].

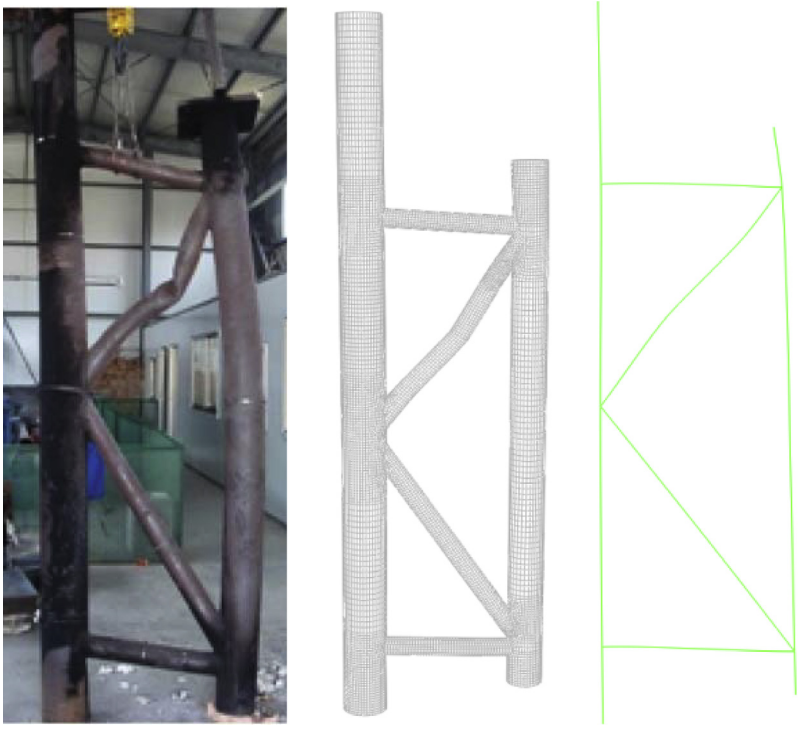

Fig. 6. Comparison of failure modes.

the truss and the simulated deformed shapes using both shell elements and line elements for the brace and chord members. The agreement between the test and simulation results is excellent. This indicates that using line elements is acceptable if failure of the truss is due to member, not joint, failure. Fig. 7 compares the detailed simulation displacement-temperature curves with the test results of Liu et al. [8]. From the comparison, it can be seen that both the four-noded shell elements and line elements give close prediction of the test results. The maximum temperatures, at which the truss is no longer able to support the applied loads, from the test, from the simulations using shell elements and using line elements are 678 °C, 642 °C and 636 °C respectively. This agreement is acceptable.

2.3.2. Girder B of Edwards [16]

Fig. 8 shows the recorded temperatures in the different truss members.

Fig. 9 compares the displacement-temperature curves at the centre point of the top chord member. The agreement with the test result is excellent for using both the line and shell elements.

The failure mode of the truss, obtained from the test, from the simulations using shell elements and using line elements was due to buckling of the middle diagonal compressive brace members (members 8 and 9 in Fig. 1) at 606 °C, 602 °C and 595 °C respectively. Fig. 10 compares the simulated and observed failure modes. It is clear that the numerical simulation model, either using 2D line elements or 3D shell elements, is suitable for simulating the overall behaviour of welded tubular trusses in fire. However, from a computational point of view, using line elements is preferable because the simulation was very fast. The line element model was used to conduct the parametric study in the next sections.

3. Influential factors on structural behaviour of truss at elevated temperature

The behaviour of a truss at elevated temperatures is affected by many design factors as well as design assumptions. The parametric study in Section 4 of this paper will investigate, in detail, the effects of different design factors. This section will present the results of a number of numerical investigations to examine the effects of different design assumptions. These assumptions are:

(1) Joints: the welded truss joint may be considered to be rigid (Fig. 11a), pinned (Fig. 11c) or semi-rigid (where the chord members are continuous, but the brace members are pinned, Fig. 11b).
(2) This investigation was to assess whether restraint to some differential thermal elongation of the members due to some temperature difference would cause any difference in truss member critical temperatures.

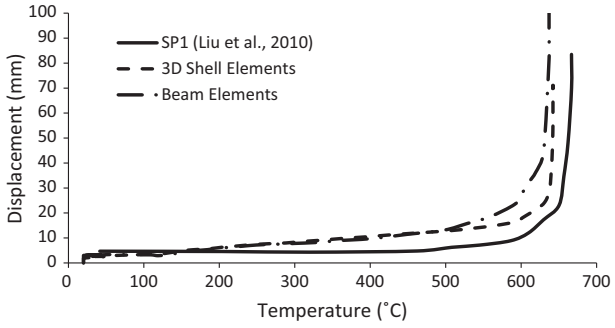

Fig. 7. Comparison for displacement-temperature curves of SP1 [8].

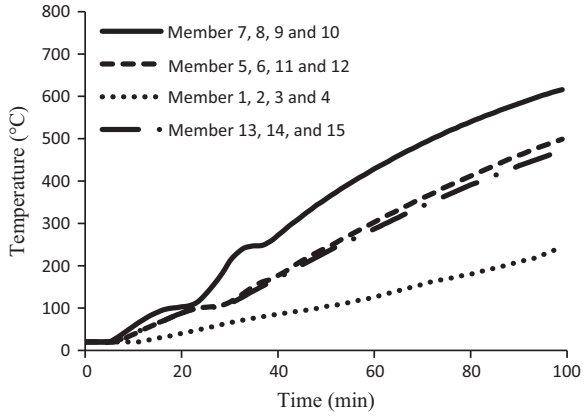

Fig. 8. Temperature–time curves of test Girder B [16].

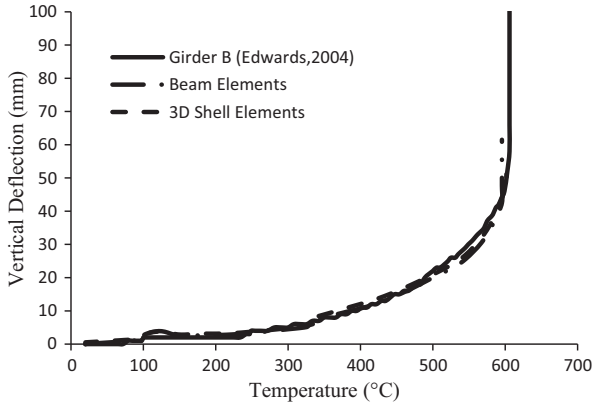

Fig. 9. Comparison for displacement-temperature curves of Girder B of Edwards [16].

Fig. 11 illustrates the joint and boundary conditions of the trusses. Table 2 list the truss member dimensions. The material strength of steel was f_y = 355 N/mm^2 f_u = 443.75 N/mm^2. The elastic modulus of steel was assumed to be 210 GPa. The elevated temperature stress–strain curves and the thermal expansion coefficient of steel were based on Eurocode EN-1993-1-2 [2].

For comparison, ABAQUS simulations of the individual truss members were carried out to obtain the critical temperatures of all the members according to the current member based design method. In these analyses, the member forces were from the same as those at 20 °C. Table 3 summarises the critical temperatures of the individual members.

In the truss simulations, the rates of temperature rise of all the members were assumed to be in proportion to their individual critical temperatures in Table 3. Whether or not thermal expansion was not considered, the truss failure temperatures were almost identical. This indicates that any differential thermal elongation due to different truss members being heated to different temperatures had negligible effect on the failure temperature of the trusses. The failure temperatures of the trusses with rigid, semi-rigid and pinned joints are 535 °C, 529 °C and 523 °C respectively.

Since assuming pinned joints gives the lowest truss failure temperature, it is suggested that this assumption may be made in fire resistant design of the truss. However, even assuming pin-joints, the member-based calculation method of using the ambient temperature forces may not be safe. For example, for the truss in Fig. 11, the member-based critical temperature of member 7 of the truss, obtained numerically using ABAQUS, was 558 °C. This

(a) Test observation [16]

(b) Failure mode using shell elements

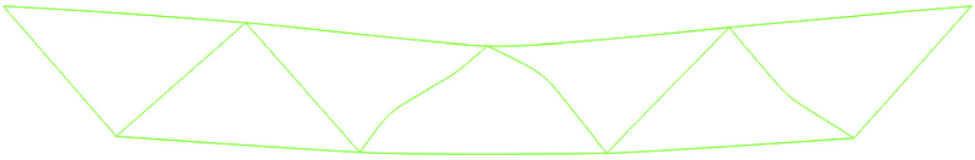

(c) Failure mode using line elements

Fig. 10. Comparison of failure modes for test Girder B of Edwards [16].

is higher than the actual critical temperature (535 °C) of the member in the rigid truss.

The reason for this difference in the critical temperature of member 7 between using the member-based method and using truss analysis is due to the increased member force in the member in truss analysis when the truss deflection is high. To confirm this, static structural analysis was performed using the deformed configuration of the truss. The initial member forces, the member force at truss failure (523 °C) and the member force from static analysis based on the deformed shape of the truss were 184.4 kN, 213.6 kN and 213.6 kN respectively.

Furthermore, the ABAQUS model of member 7 was rerun, in this case using the final member forces (213.6 kN), and the failure temperature was 523 °C, exactly the same as the failure temperature of the member in the pin-jointed truss.

Parametric study will investigate how the member forces change and the effects of this change on member critical temperatures. In the investigations, the truss will be assumed to be pin-jointed.

4. Parametric study

Extensive numerical simulations have been conducted on Warren, Howe and Pratt trusses. Fig. 12 shows the different types of the trusses being investigated and the following explains the rationale for selecting the different parameters:

Case 1, span-to-depth ratio (Warren truss, see Fig. 13): different span to depth ratios will give different chord axial force values and different diagonal member angles.
Case 2, member slenderness, λ (varying from 48 to 89, Warren and Pratt trusses): to investigate different member failure modes.
Case 3, applied load ratio, (Warren truss with a span of 25 m and Pratt truss with a span of 12 m): to investigate the effect of changing chord force.
Case 4, truss span: Warren truss, span of 4.5 m, 12 m and 25 m.
Case 5, truss configurations: Warren, Howe and Pratt trusses (see Fig. 12).
Case 6, number of braces: Warren truss with a span of 12 m. Three different configurations were modelled as shown in Fig. 16. The total applied load and angle between brace and chord members were constant.
Case 7, failure location: Pratt truss with a span of 100 m. The dimensions of the outer and inner brace members were changed to move location of the critical member.

Appendix A gives the cross-sectional dimensions use in the simulations.

4.1. Simulation results and discussions

4.1.1. Case 1: effect of span-to-depth ratio

Fig. 13 illustrates the geometric configurations of the Warren trusses with different span-depth ratios. Table A.1 summarises the member dimensions of the trusses used in the parametric study and Table 4 provides a summary of the simulation results. In Table 4, P_θ/P_{20} is the ratio of the member force at elevated temperature (P_θ) from truss analysis to that at ambient temperature (P_{20}). In all cases, failure was initiated in member 7. The member based analysis gives a critical temperature of more than 30 °C higher than truss analysis for truss span to depth ratio of 18.

As the span to depth ratio increases, the angles between the chord and brace members become smaller. As will be shown in Section 5 which presents a method to calculate the increased member force in compressive diagonal member, it is the vertical component of the chord force in the deformed truss that increases the compression force in the diagonal brace members. This increase is in inverse relationship to the angle between the diagonal brace member and the chord member. A smaller angle (for large truss span to depth ratio) leads to a higher increase in the brace member force.

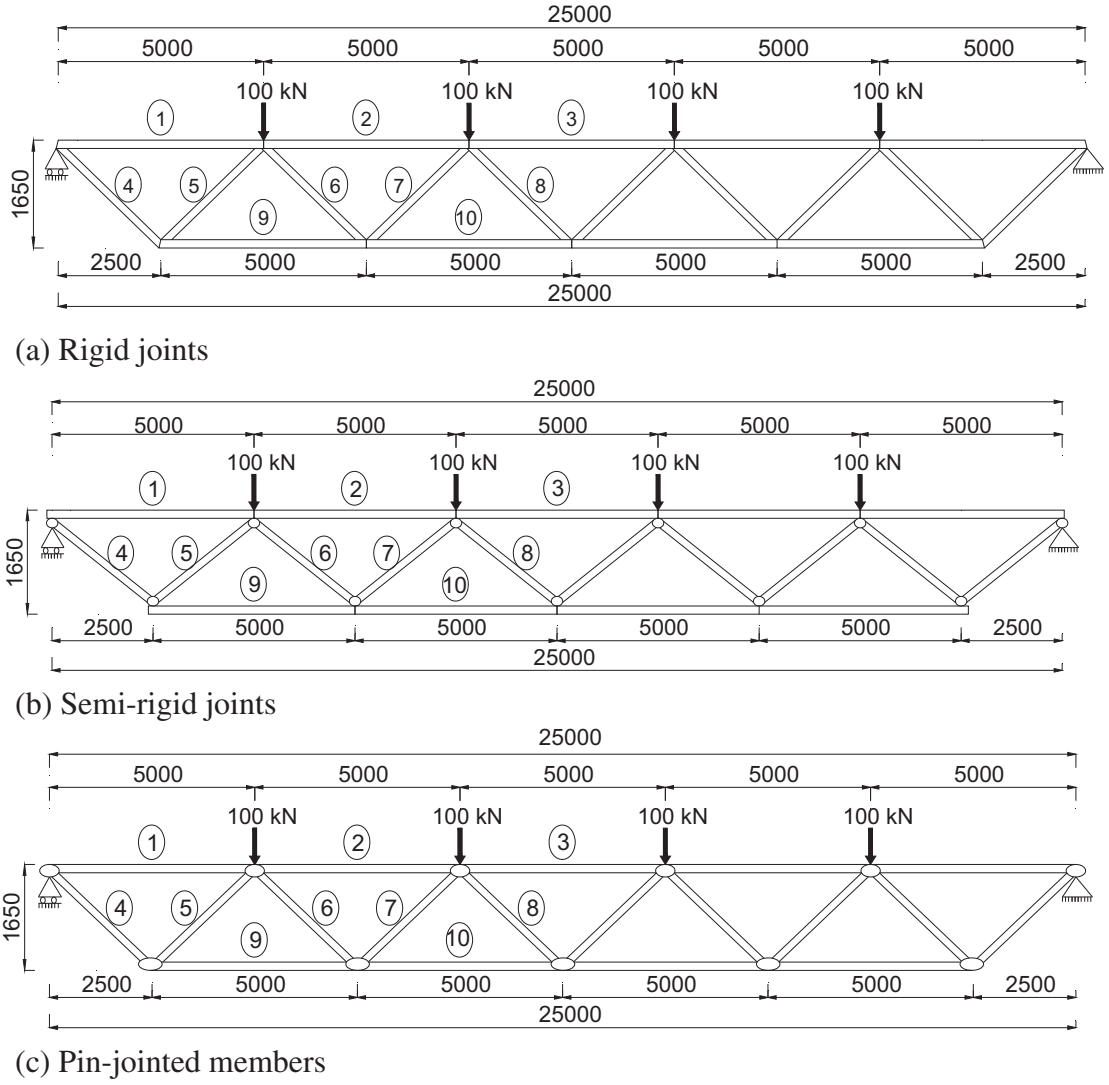

Fig. 11. Truss configurations used in numerical analyses (dimensions in mm).

Table 2
Truss member dimensions.

Member Type	Dimensions (mm)
Bottom and top chords	∅323.9 × 8
Outer bracings (Member 4 and 5)	∅193.7 × 4
Inner bracings (Member 6, 7 and 8)	∅114.3 × 5

4.1.2. Case 2: Effect of member slenderness (λ)

This case used the Warren truss shown in Fig. 13b and the Pratt truss shown in Fig. 12c. The influence of different slenderness values for the Warren truss ($\lambda = 89$, 78 and 62) was examined by changing the cross section of critical member 7 (∅101.6 × 6.3, ∅114.3 × 5 and ∅139.7 × 3 respectively for the above slenderness values). In the case of the Pratt truss, the critical member was member 10 and the member size was ∅76.1 × 2.5, ∅60.3 × 3.6 and ∅48.3 × 5 to give slenderness values of $\lambda = 48$, 62 and 81 respectively.

Tables 5 and 6 summarise the simulation results for the Warren and Pratt trusses respectively. Because the overall geometry of the trusses was unchanged, the truss member forces were similar in all cases. However, a comparison between Tables 5 and 6 shows that the increase in member force in the Pratt truss is greater. This is expected because the increase in the compression force (due to the vertical component of the compression chord force in the deformed position of the truss) of the brace is shared by two diagonal members in the Warren truss but resisted by only one single member in the Pratt truss.

4.1.3. Case 3: effect of applied load ratio

For this investigation, the Warren truss in Fig. 13b and the Pratt truss in Fig. 12c were used. Each point load was 50 kN. Table 7 presents the simulation results. The member forces change similarly

Table 3
Critical temperatures of the individual members of the Warren truss in Fig. 11c.

Member no	1	2	3	4	5	6	7	8	9	10
Critical temperature (°C)	780	652	624	577	573	640	545	635	679	624

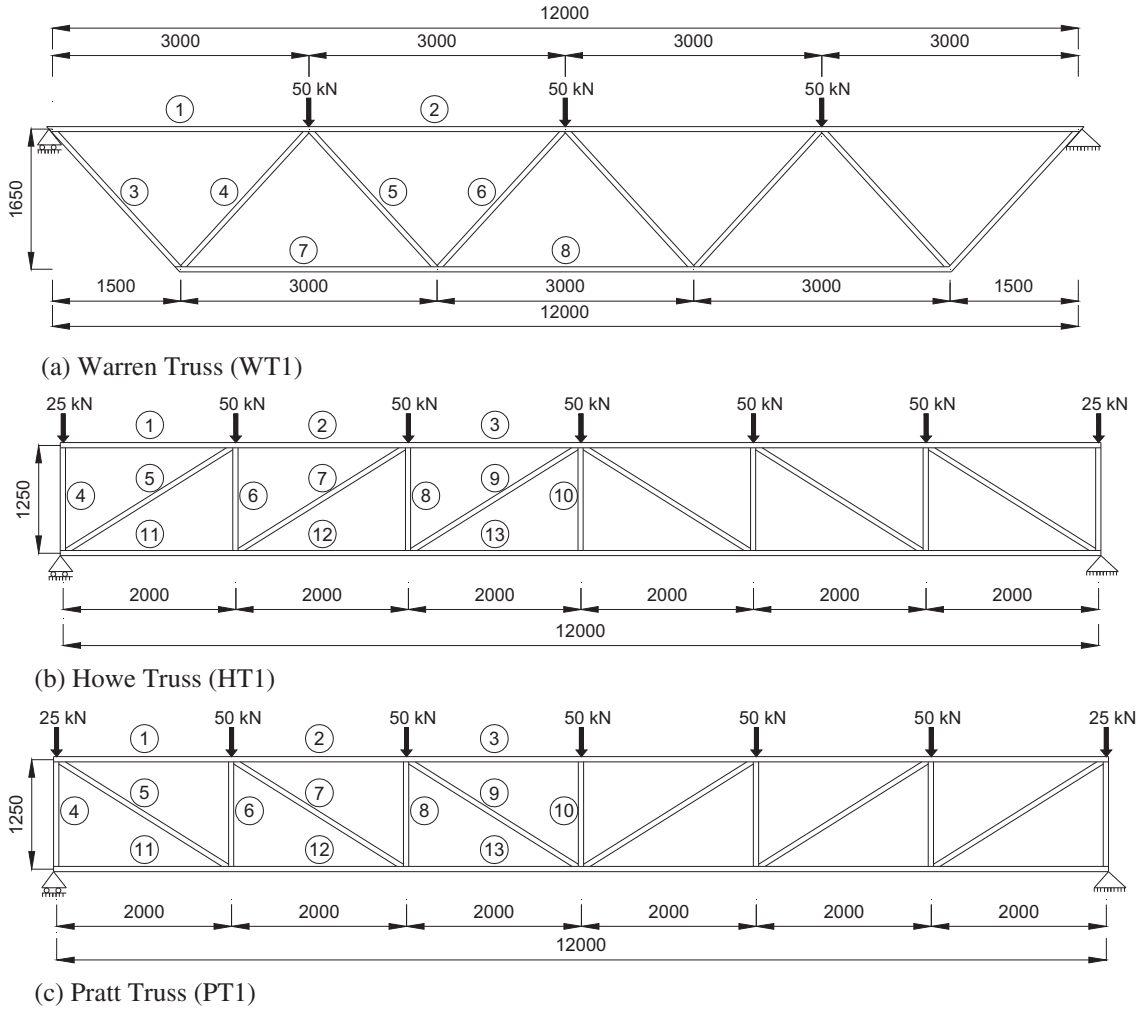

Fig. 12. Truss configurations used in parametric study (dimensions in mm).

as discussed in the previous section. However, the effect of the same change in the member compression force is different at different load ratios. For the Pratt truss with a high load ratio (applied load = 100 kN), the reduction of truss critical temperature from the member based analysis is nearly 60 °C.

4.1.4. Case 4: effect of truss span

In this investigation, the span of a Warren truss was changed but the span to depth ratio was kept constant at 20.8. Fig. 14 shows the truss dimensions.

Table 8 compares the simulation results. Since the span to depth ratio was constant, the member forces experienced very similar changes. Due to the shallow truss depth, the increase in member force was quite high, resulting in truss critical temperatures much lower (by as much as 76 °C) than that from member based analysis.

4.1.5. Case 5: effect of truss configuration

Warren, Howe and Pratt trusses of the same span, the same span-to-depth ratio and the same load level were simulated. Fig. 12 shows the truss dimensions.

Table 9 compares the simulation results. Fig. 15 shows the members that experienced increase in their compression forces to resist the vertical component of the chord forces in the deformed condition. As expected, the more brace members are involved in sharing the load (Howe truss > Warren truss > Pratt truss), the lower increase in the compression force of each member are obtained.

The results of this investigation show that the effect of increased member force may be ignored for Howe trusses. In the case of increased member forces, Pratt truss analysis revealed a more significant effect on the failure temperature compared to Warren trusses. This effect should be considered for fire resistance analysis of both Warren and Pratt trusses when failure takes place in the middle brace members.

4.1.6. Case 6: effect of number of braces

For this investigation, the trusses in Fig. 16 were used. The number of brace members was different, all other dimensions being equal. The total load was 500 kN.

Table 10 compares the simulation results. Changing the number of brace members in a truss changes the maximum chord compression force. As the number of brace members increases, the chord compression force at the truss centre increases. This increase in the chord compression force results in a higher increase in the brace compression force. For truss A, which is sensibly proportioned, the brace compression force at truss failure more than doubled the initial compression force. This resulted in a truss critical temperature of more than 100 °C lower than the member based result which did not include this increase in the brace force.

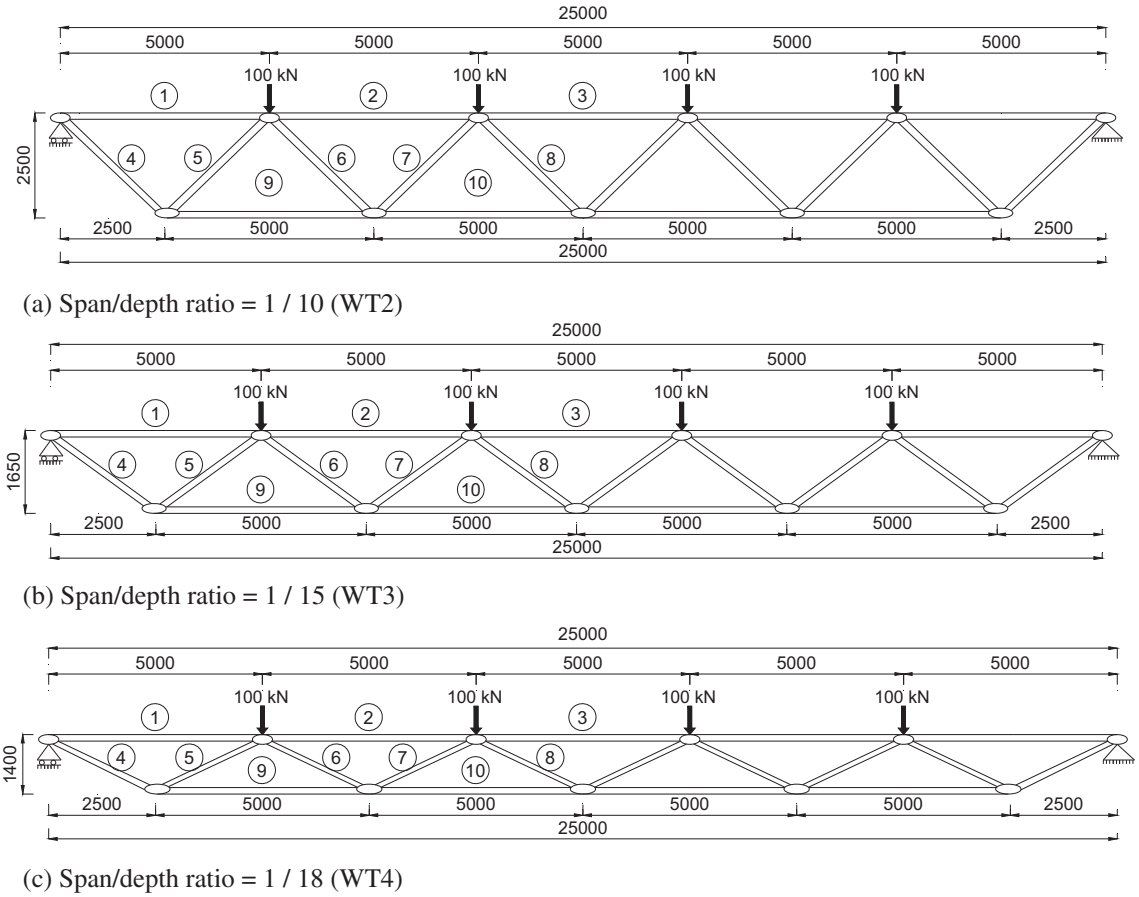

Fig. 13. Warren trusses with different span/depth ratios (dimensions in mm).

Table 4
Effect of truss span to depth ratio on critical temperature.

		Isolated Member 7	Heated Truss
Depth Ratio : 1/10	Critical temperature	556 °C	540 °C
	Maximum displacement	–	389 mm
	Member force ratio (P_θ/P_{20})	1.00	1.07
Depth Ratio : 1/15	Critical temperature	558 °C	523 °C
	Maximum displacement	–	587 mm
	Member force ratio (P_θ/P_{20})	1.00	1.19
Depth Ratio : 1/18	Critical temperature	541 °C	509 °C
	Maximum displacement	–	663 mm
	Member force ratio (P_θ/P_{20})	1.00	1.22

Table 5
Effect of member slenderness on Warren truss critical temperature.

		Isolated Member 7	Heated Truss
λ = 89	Critical temperature	532 °C	508 °C
	Maximum displacement	–	563 mm
	Member force ratio (P_θ/P_{20})	1.00	1.16
λ = 78	Critical temperature	558 °C	523 °C
	Maximum displacement	–	587 mm
	Member force ratio (P_θ/P_{20})	1.00	1.19
λ = 62	Critical temperature	547 °C	518 °C
	Maximum displacement	–	574 mm
	Member force ratio (P_θ/P_{20})	1.00	1.16

Table 6
Effect of member slenderness on Pratt truss critical temperature.

		Isolated Member 10	Heated Truss
λ = 81	Critical temperature	602 °C	579 °C
	Maximum displacement	–	210 mm
	Member force ratio (P_θ/P_{20})	1.00	1.23
λ = 62	Critical temperature	650 °C	618 °C
	Maximum displacement	–	222 mm
	Member force ratio (P_θ/P_{20})	1.00	1.26
λ = 48	Critical temperature	656 °C	609 °C
	Maximum displacement	–	260 mm
	Member force ratio (P_θ/P_{20})	1.00	1.30

4.1.7. Case 7: effect of failure location

In the previous cases, failure of the truss was initiated in the brace near the centre of the truss. In this simulation, failure of the truss was forced to start from the brace member near the support by reducing the size of this member. A Pratt truss with a span of 100 m was used and Fig. 17 shows the truss dimensions.

Table 11 compares the results between the two failure locations. When the failure is near the support, using truss analysis gave the same results as the member based analysis. This is because the increase in the brace force was very small, a result of small chord compression force and small change in the line of action in the chord compression force (as will be explained in Section 5).

Table 7
Effects of applied load ratio on Warren and Pratt truss critical temperatures.

		Warren truss		Pratt truss	
		Isolated Member 7	Heated Truss	Isolated Member 10	Heated Truss
Applied load: 50 kN	Critical temperature	655 °C	630 °C	656 °C	609 °C
	Maximum displacement	–	630 mm	–	260 mm
	Member force ratio (P_θ/P_{20})	1.00	1.18	1.00	1.30
Applied load: 100 kN	Critical temperature	558 °C	523 °C	556 °C	498 °C
	Maximum displacement	–	587 mm	–	240 mm
	Member force ratio (P_θ/P_{20})	1.00	1.19	1.00	1.29

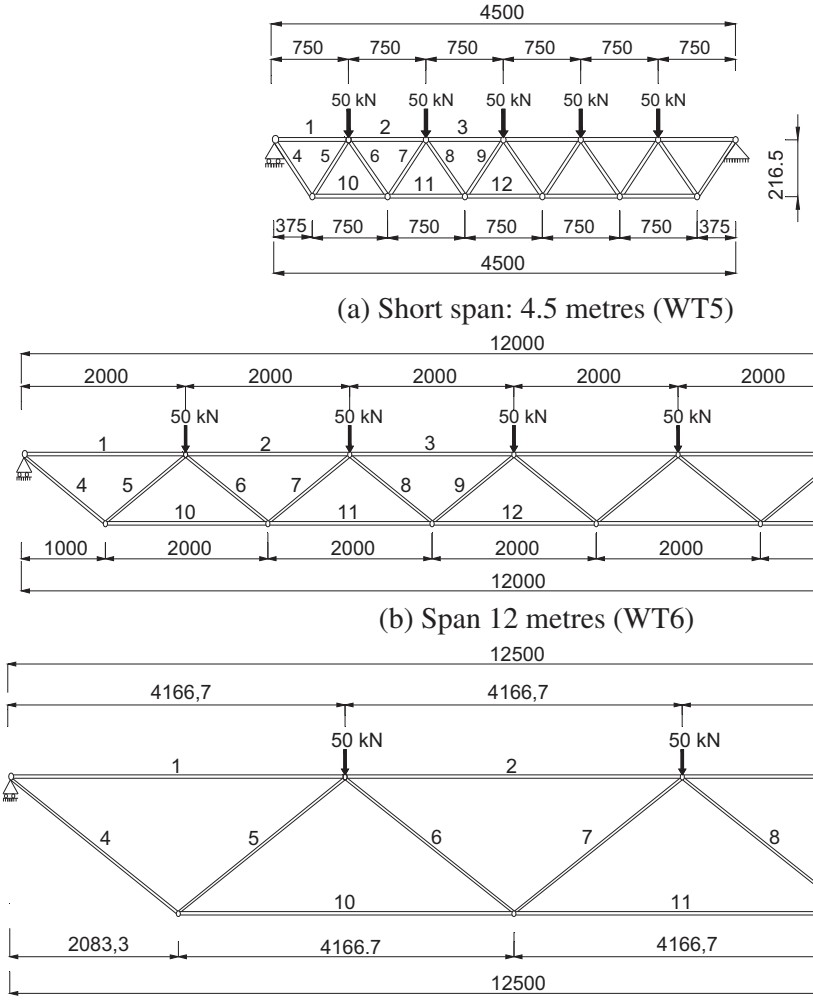

Fig. 14. Dimensions of Warren trusses with different spans (dimensions in mm).

Table 8
Effect of truss span with constant span to depth ratio.

	Span: 4.5 m		Span: 12 m		Span: 25 m	
	Isolated Member 9	Heated Truss	Isolated Member 9	Heated Truss	Isolated Member 9	Heated Truss
Critical temperature	635 °C	586 °C	647 °C	571 °C	624 °C	575 °C
Maximum displacement	–	97 mm	–	221 mm	–	532 mm
Member force ratio (P_θ/P_{20})	1.00	1.33	1.00	1.35	1.00	1.32

Table 9
Effects of truss configuration.

	Warren truss		Howe truss		Pratt truss	
	Isolated Member 9	Heated Truss	Isolated Member 9	Heated Truss	Isolated Member 9	Heated Truss
Critical temperature	652 °C	636 °C	644 °C	640 °C	656 °C	609 °C
Maximum displacement	–	168 mm	–	378 mm	–	260 mm
Member force ratio (P_θ/P_{20})	1.00	1.12	1.00	1.03	1.00	1.30

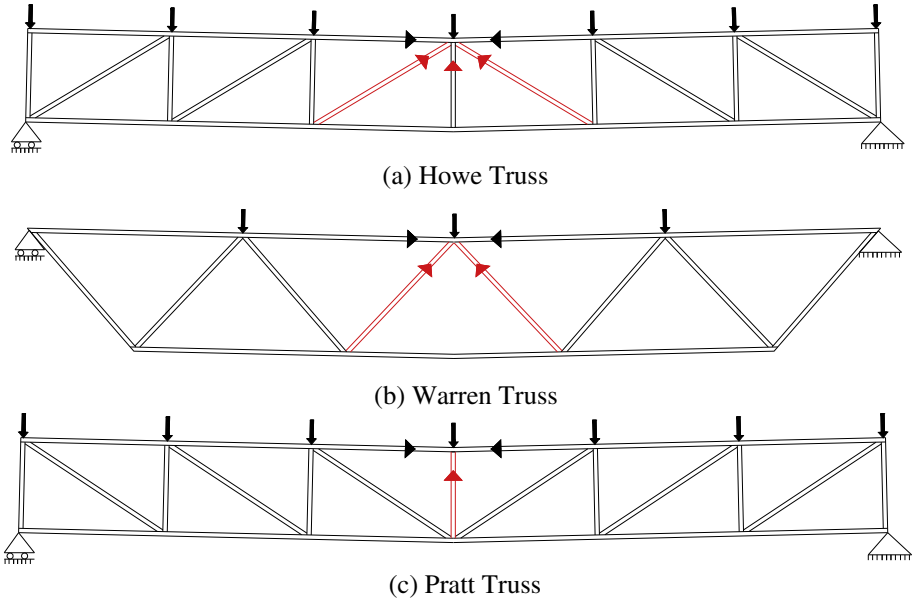

Fig. 15. Deformed shape of truss.

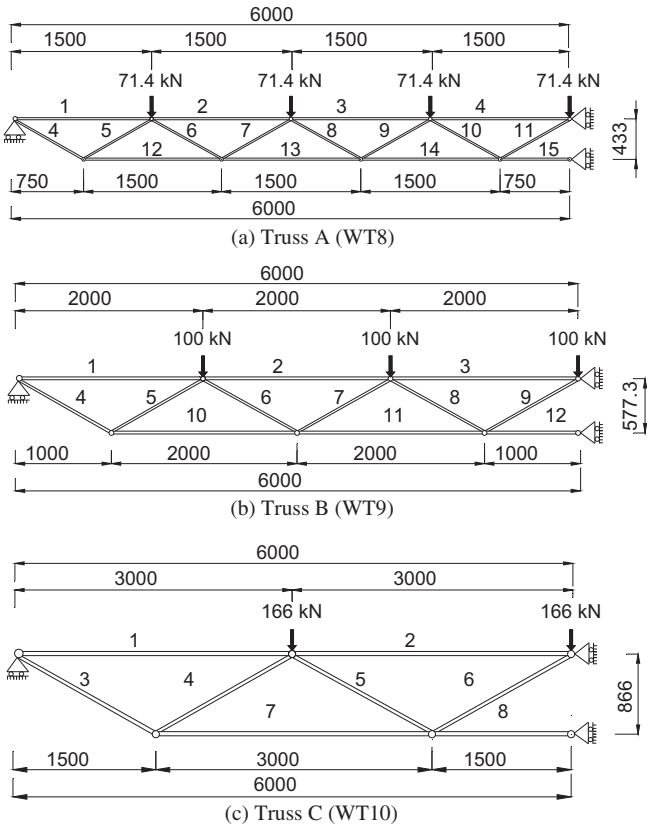

Fig. 16. Dimensions of Warren trusses (half span, dimensions in mm).

4.2. Summary of results

In summary, these results show that due to truss undergoing large displacements at elevated temperatures, some truss members (compression brace members near the truss centre) experience large increases in member forces. Therefore, when calculating the member critical temperatures, it would not be safe to use the member forces from ambient temperature structural analysis. Using the ambient temperature member force may overestimate the truss member critical temperature (based on truss analysis) by 100 °C.

The influence of slenderness on the truss member forces was ignorable owing to the unchanged overall geometry of the trusses. Also, span of the trusses had no effect on the critical temperature as long as the span to depth ratio was constant.

As will be explained in the next section, the changes in forces in the top chord, bottom chord and tension brace members of Howe, Pratt and Warren trusses are small at high temperatures. However, the effect of the deformed shape of Pratt and Warren trusses at elevated temperatures on the compression brace members is considerable. Furthermore, the angle between diagonal member and chord member has a significant influence on failure temperature of the trusses.

5. Development of a simple method

The lower truss critical temperatures from truss analysis compared to member based analysis are a result of increased brace compression force. A method will be developed in this section to calculate this force increase. This increase is a result of the large deflection of the truss. As shown in Table 12, the maximum truss

Table 10
Effects of number of brace members.

	Truss A		Truss B		Truss C	
	Isolated Member 11	Heated Truss	Isolated Member 9	Heated Truss	Isolated Member 6	Heated Truss
Critical temperature	746 °C	642 °C	692 °C	623 °C	597 °C	542 °C
Maximum displacement	–	183 mm	–	227 mm	–	218 mm
Member force ratio (P_θ/P_{20})	1.00	2.07	1.00	1.70	1.00	1.36

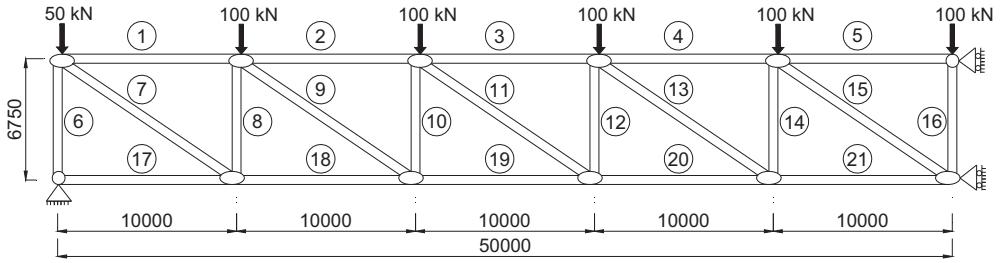

Fig. 17. Dimensions of a Pratt truss (half span shown, dimensions in mm), (PT2).

Table 11
Effects of the failure location.

	Inner brace failure		Outer brace failure	
	Isolated Member 16	Heated Truss	Isolated Member 6	Heated Truss
Critical temperature	566 °C	515 °C	585 °C	590 °C
Maximum displacement	–	1417 mm	–	3033 mm
Member force ratio (P_θ/P_{20})	1.00	1.40	1.00	0.99

deflection ranged from 0.014 to 0.03 of the truss span (span to deflection ratios of 71 and 33 respectively). In the fire protection industry, a deflection limit of span/30 is often used [20] to determine fire resistance. For simplicity and for safety, this value will be used in developing the calculation method.

To enable detailed comparison for forces in different truss members between calculation using the proposed analytical method and truss analysis results, results for the Warren and Pratt trusses shown in Fig. 18 are used.

The critical temperature of the Warren truss was 623 °C, due to buckling of brace member 9 in compression. At truss failure, the maximum truss deflection was 293 mm. Tables 13 and 14 compare the truss member forces with their initial values at 20 °C. For the Pratt truss, the critical temperature was 617 °C, reached due to failure of member 16. At the failure temperature, the maximum truss deflection was 638 mm.

The results in Tables 13 and 14 reveal the following trend clearly:

- Forces in the tension brace members decrease. Therefore, for these members, the current member based design method is on the safe side.
- The changes in forces in the chord members are small. Therefore, the current member based design method is acceptable.
- The large percentage change in forces occurs in the compression brace members near the centre of the truss. Away from the truss centre, the change in compression force in the brace members rapidly diminishes.

Table 12
Maximum truss deflections.

Member No	δ_{max} (mm)	L (mm)	δ_{max} (L)
WT1	168	12,000	0.014
WT2	389	25,000	0.016
WT3-A	587	25,000	0.024
WT3-B	563	25,000	0.023
WT3-C	574	25,000	0.023
WT3-D	630	25,000	0.025
WT4	663	25,000	0.027
WT5	97	4500	0.022
WT6	221	12,000	0.018
WT7	523	25,000	0.021
WT8	183	12,000	0.015
WT9	227	12,000	0.019
WT10	218	12,000	0.018
PT1-A	210	12,000	0.018
PT1-B	222	12,000	0.019
PT1-C	260	12,000	0.022
PT1-D	240	12,000	0.02
PT2-A	1417	100,000	0.014
PT2-B	3033	100,000	0.03
PT3	638	25,000	0.026

5.1. Maximum increase in compression brace force at centre of truss

Refer to Fig. 19 which shows the deformed geometry at the joint at the centre of the truss, the increase in compression force in the compression brace members (member 9) is to resist the vertical components of the compression chords (member 3).

Assuming the maximum truss deflection is δ. The angle between the straight line drawn from the support to the maximum deformed position of the compression chord is $\alpha = \delta/(L/2)$ where L is the total span of the truss. The angle between the deformed compression chord and the horizontal is approximately $\alpha/2$. Based on the above assumptions, the additional vertical force from one of the two chord members with the maximum compression force (chord member 3) can be calculated as:

$$F_{maximum\ chord\ compression} * \frac{\delta}{L/2} * \frac{1}{2} = F_{maximum\ chord\ compression} * \frac{\delta}{L} \quad (3)$$

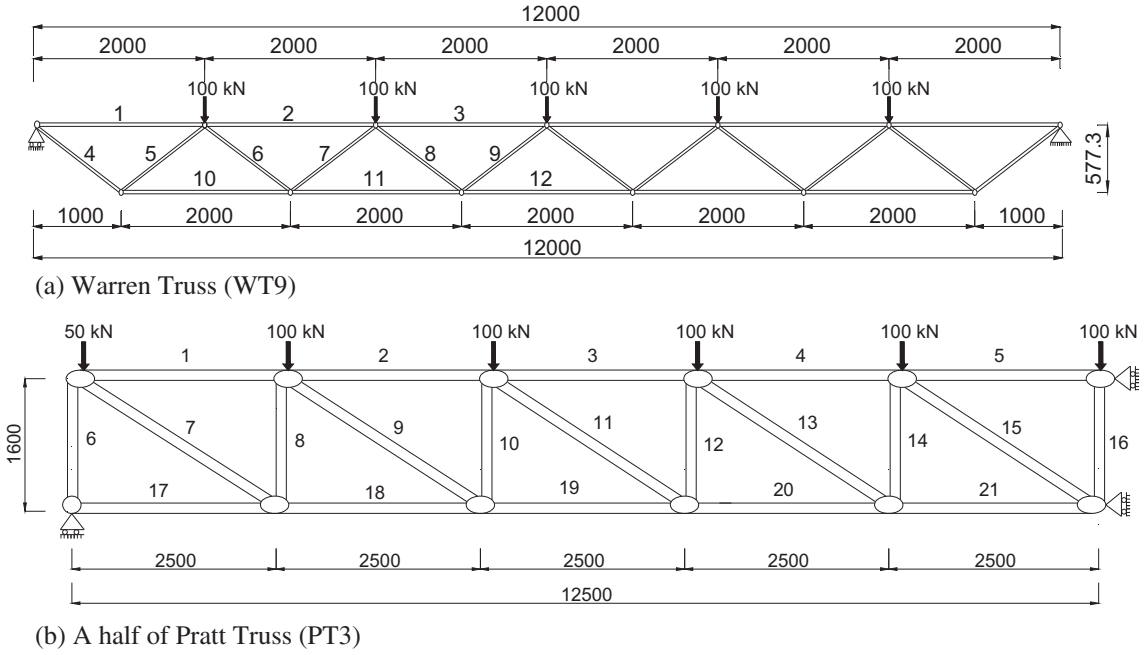

Fig. 18. Dimensions of trusses used for detailed comparison of additional forces (dimensions in mm).

Table 13
Comparisons of the member forces for the Warren truss in Fig. 18 (unit in kN).

Member No	ABAQUS		
	$F_{20^\circ C}$	$F_{max,\ Abaqus}$	Ratio ($F_{max,\ Abaqus}/F_{20^\circ C}$)
1	−433.0	−416.2	0.96
2	−1125.8	−1107.8	0.98
3	−1472.0	−1462.7	0.99
4	500.0	501.6	1.00
5	−500.0	−512.4	1.02
6	300.0	274.4	0.91
7	−300.0	−345.5	1.15
8	100.0	57.6	0.58
9	**−100.0**	**−167.1**	**1.67**
10	866.0	878.7	1.01
11	1385.6	1414.5	1.02
12	1558.8	1608.4	1.03

Bold indicates the critical member.

Table 14
Comparisons of the member forces for the Pratt truss in Fig. 18 (unit in kN).

Member No	ABAQUS		
	$F_{20^\circ C}$	$F_{max,\ Abaqus}$	Ratio ($F_{max,\ Abaqus}/F_{20^\circ C}$)
1	−703.1	−713.0	1.01
2	−1250.0	−1267.5	1.01
3	−1640.6	−1655.3	1.01
4	−1875.0	−1891.1	1.01
5	−1953.1	−1987.0	1.02
6	−500.0	−498.8	1.00
7	834.8	851.4	1.02
8	−450.0	−453.7	1.01
9	649.3	658.1	1.01
10	−350.0	−365.4	1.04
11	463.8	460.6	0.99
12	−250.0	−284.1	1.14
13	278.2	279.1	1.00
14	−150.0	−186.0	1.24
15	92.8	92.5	1.00
16	**−100.0**	**−189.6**	**1.90**
17	0.0	23.7	–
18	703.1	732.4	1.04
19	1250.0	1278.2	1.02
20	1640.6	1660.0	1.01
21	1875.0	1892.3	1.01

Bold indicates the critical member.

Therefore, the maximum increase in compression force in the brace member (member 9) can be calculated as follows:

$$\Delta F_{truss\ centre} = F_{truss\ centre,0} + \frac{F_{maximum\ chord\ compression} * \frac{\delta}{L}}{\sin\theta} \quad (4)$$

where θ is the angle between the compression brace member at the truss centre (member 9) and the horizontal.

The total compressive force in the brace member at the truss centre (member 9) is:

$$F_{truss\ centre} = F_{truss\ centre,0} + \frac{F_{maximum\ chord\ compression} * \frac{\delta}{L}}{\sin\theta} \quad (5)$$

5.2. Increase in compression brace force away from the centre of truss

Away from the centre of truss, the increase in force in the compression brace members decrease rapidly for three reasons: (1) the chord compression force are lower; (2) the additional vertical force from one of the two chord members with the higher compression force are shared by two brace members; (3) as shown in Fig. 19(c), the relative chord rotation (γ) between two adjacent members is much smaller than angle $\alpha/2$ to the horizontal at the centre of the truss (Fig. 19(b)). Because the percentage increases in forces in these members are small, gross approximation is acceptable when calculating the force increase in these members. Assuming the chord compression force decreases linearly from at the truss centre to 0 at support, and assuming that the relative rotation of the chord members at each node is $\alpha/2$, the increase in compression force in compression brace members not at the centre of the truss can be approximately calculated as:

$$\Delta F_{other\ brace\ member} = \frac{1}{2} * \Delta F_{trusscentre} * \frac{d}{L/2} \quad (6)$$

where is d is the distance from the support to the node connecting the compression brace member whose force is calculated.

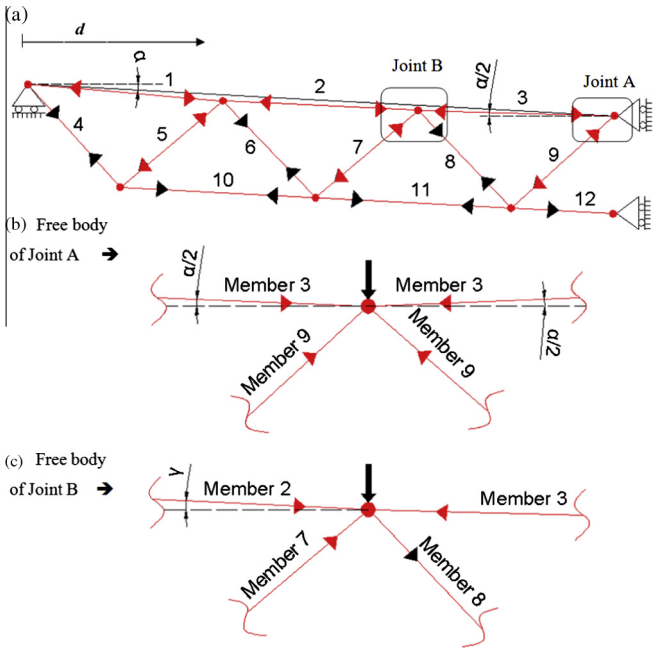

Fig. 19. Deformed shape and free body diagrams for a Warren truss.

$$F_{other\ brace\ member} = F_{other\ brace\ member,0} + \frac{1}{2} * \Delta F_{truss\ centre} * \frac{d}{L/2} \quad (7)$$

For the Pratt truss, as shown in Fig. 18, because there is only one vertical member at the centre, the additional compressive force is twice as given in Eq. (5) and $\theta = 90°$. Therefore:

$$\Delta F_{truss\ centre} = 2 * F_{maximum\ chord\ compression} * \frac{\delta}{L} \quad (8)$$

The increase in compression force in the members away at the centre can be calculated using Eq. (7) for the same reasoning as for the Warren truss.

Tables 15 and 16 compare the compression brace forces from truss analysis ($F_{max,\ Abaqus}$) with those calculated using Eqs. 5, 7 and 8 for the two trusses, one for the actual maximum truss deflection at failure (F_{max}) and one for the assumed maximum truss deflection of $L/30$ ($F_{assumed}$). As can be seen from the tables below, the predicted forces in compression brace members are slightly higher, but reasonably close to the member forces based on truss numerical simulations.

The accuracy of the proposed analytical method has been checked against all the simulation trusses which were used in the parametric study. Fig. 20 compares the maximum compression brace forces at the centre of the trusses from truss analysis with those calculated using Eqs. (5) and (8) for two maximum truss deflections: the maximum truss deflection at failure from ABAQUS analysis and the assumed maximum truss deflection of $L/30$. Also, original truss member forces at 20 °C ($F_{20°C}$) are included in Fig. 20.

Table 15
Comparisons of compressive member forces for the Pratt truss in Fig. 18 (unit in kN).

Member No		ABAQUS	Eqs. (7) and (8)			
	$F_{20°C}$	$F_{max,\ Abaqus}$	ΔF_{max}	F_{max}	$\Delta F_{assumed}$	$F_{assumed}$
8	−450.0	−453.7	−3.6	−453.6	−4.7	−454.7
10	−350.0	−365.4	−12.8	−362.8	−16.7	−366.7
12	−250.0	−284.1	−25.1	−275.1	−32.8	−282.8
14	−150.0	−186.0	−38.3	−188.3	−50.0	−200.0
16	**−100.0**	**−189.6**	**−99.7**	**−199.7**	**−130.2**	**−230.2**

Bold indicates the critical member.

Table 16
Comparisons of compressive member forces for the Warren truss in Fig. 18 (unit in kN).

Member no.		ABAQUS	Eqs. (5) and (7)			
	$F_{20°C}$	$F_{max,\ Abaqus}$	ΔF_{max}	F_{max}	$\Delta F_{assumed}$	$F_{assumed}$
WT9-M5	−500.0	−508.0	−5.5	−505.5	−9.6	−509.6
WT9-M7	−300.0	−330.2	−28.4	−328.4	−50.0	−350.0
WT9-M9	**−100.0**	**−169.6**	**−55.7**	**−155.7**	**−98.1**	**−198.1**

Bold indicates the critical member.

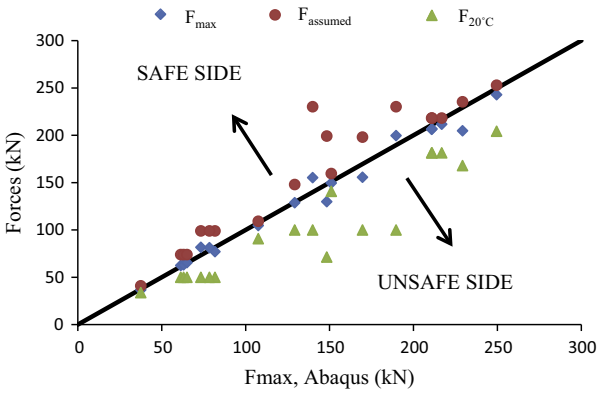

Fig. 20. Comparison for forces in critical members of Warren and Pratt trusses between analytical calculations, ABAQUS simulation results and ambient temperature values.

The results in Fig. 20 indicate that the proposed calculation method can produce very accurate results if the actual maximum deflection of truss is used. If a value of $L/30$ is used for the maximum deflection, the calculation results are reasonably close to the ABAQUS simulation results, and are on the safe side. In contrast, using the ambient temperature forces can greatly underestimate the member forces and produce unsafe design.

Fig. 21 illustrates the same comparisons for other compression brace members. Because the ambient temperature forces are high and the associated chord member forces are small, the changes in these member forces are much smaller than for the critical members shown in Fig. 20. Therefore, the three sets of results are much closer to each other than shown in Fig. 20. Nevertheless, using the ambient temperature member forces is unsafe in some cases. Since the proposed calculation method is simple to use and the calculation results are in good agreement with the ABAQUS simulation results, it is recommended using the proposed analytical method.

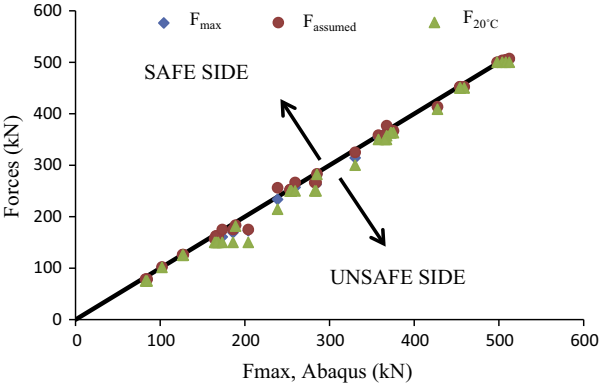

Fig. 21. Comparison for forces in compression brace members of Warren and Pratt trusses between analytical calculations, ABAQUS simulation results and ambient temperature values.

6. Conclusions

This paper has presented the results of a numerical investigation into the behaviour of welded steel tubular truss at elevated temperatures. Finite Element (FE) simulations were carried out for Circular Hollow Section (CHS) trusses using the commercial Finite Element software ABAQUS v6.10-1 [1]. Finite Element (FE) simulations of tubular steel trusses at elevated temperatures were first validated against available test results of Edwards [16] and Liu et al. [8].

The focus of this paper was truss behaviour and how truss action can be taken into account when calculating truss member critical temperatures. It has been found that when calculating truss member critical temperatures, the joints between truss members may be safely simplified as pin joints. This simplification allows ignoring the effects of any differential thermal expansion in different truss members.

The main conclusion of the parametric study on truss behaviour was that the member-based calculation method for calculating member critical temperatures, in which the ambient temperature truss member forces are used, may not be safe. The critical temperature from the present member based calculation method can overestimate the truss critical temperature by as much as 100 °C. The reason for this is that compression brace members experience increases in their forces at large truss deflections. The increase in compression brace member force is the highest at the centre of the truss and rapidly decreases towards the supports. The increase in compression brace member force is higher in Pratt truss than in Warren truss.

This paper has developed an analytical method to calculate increases in truss compressive brace member forces. This calculation member forces depend on the maximum truss deflection in fire. By using a maximum truss deflection of span L/30, a value that is familiar to fire protection engineers, the proposed analytical method produces results that are in reasonably good agreement with ABAQUS simulation results and are generally on the safe side.

Acknowledgement

The authors would like to acknowledge CIDECT for partially funding this project, under the CIDECT project: 5CB-Uniformly Heated Truss.

Appendix A

See Table A.1.

Table A.1
Dimensions of the trusses members.

Truss	Member type	Dimensions (mm)
WT1 & WT3	Bottom and top chords	∅323.9 × 8
	Outer bracings (Member 4 and 5)	∅193.7 × 4
	Inner bracings (Member 6, 7 and 8)	∅114.3 × 5
WT2	Bottom and top chords	∅244.5 × 8
	Outer bracings (Member 4 and 5)	∅139.7 × 8
	Inner bracings (Member 6, 7 and 8)	∅114.3 × 5
WT4	Bottom and top chords	∅323.9 × 8
	Outer bracings (Member 4 and 5)	∅168.3 × 6
	Inner bracings (Member 6, 7 and 8)	∅114.3 × 5
WT5	Bottom and top chords	∅219.1 × 12
	Outer bracings (Member 4, 5, 6 and 7)	∅168.3 × 5
	Inner bracings (Member 8 and 9)	∅48.3 × 3.2
WT6	Bottom and top chords	∅219.1 × 12
	Outer bracings (Member 4, 5, 6 and 7)	∅168.3 × 5
	Inner bracings (Member 8 and 9)	∅60.3 × 3
WT7	Bottom and top chords	∅219.1 × 12
	Outer bracings (Member 4, 5, 6 and 7)	∅168.3 × 5
	Inner bracings (Member 8 and 9)	∅88.9 × 3
WT8	Bottom and top chords	∅406.4 × 16
	Outer bracings (Member 4, 5, 6, 7, 8 and 9)	∅168.3 × 10
	Inner bracings (Member 10 and 11)	∅114.3 × 3.6
WT9	Bottom and top chords	∅406.4 × 12
	Outer bracings (Member 4, 5, 6 and 7)	∅168.3 × 10
	Inner bracings (Member 8 and 9)	∅114.3 × 3.6
WT10	Bottom and top chords	∅406.4 × 12
	Outer bracings (Member 3 and 4)	∅168.3 × 10
	Inner bracings (Member 5 and 6)	∅114.3 × 3.6
PT1	Bottom and top chords	∅193.7 × 10
	Compression brace members (Member 4, 6 and 8)	∅114.3 × 5
	Tension brace members (Member 5, 7 and 9)	∅168.3 × 6.3
	Middle brace member (Member 10)	∅76.1 × 2.5
PT2	Bottom and top chords	∅457 × 12
	Brace members	∅219.1 × 10
PT3	Bottom and top chords	∅406.4 × 16
	Member 7 and 9	∅244.5 × 12
	Member 6, 8, 10, 11, 12, 13 and 14	∅168.3 × 10
	Member 15 and 16	∅114.3 × 3
HT1	Bottom and top chords	∅193.7 × 10
	Outer bracings (Member 5, 6 and 7)	∅168.3 × 6.3
	Inner bracings (Member 4, 8 and 9)	∅76.1 × 5

References

[1] ABAQUS/Standard. In: Hibbitt KaS, editor, K. a. S. Hibbit: USA, 2011.
[2] CEN, Design of Steel Structures. In: EN 1993-1-2-Structural Fire Design, Part: Editor. 2005, British Standard Institute: London.
[3] CIDECT, Design Guide for Circular Hollow Section (CHS) Joints Under Predominantly Static Loading, ed. S. Edition. 2010, Verlag TUV Rheinland, Germany.
[4] CEN, Design of Steel Structures. In: EN 1993-1-8-Design of Joints, Part: Editor. 2005, British Standard Institute: London.
[5] Nguyen MP, Fung TC, Tan KH. An experimental study of structural behaviours of CHS T-joints subjected to brace axial compression in fire condition. in Tubular Structures XIII. CRC Press/Balkema, 2010.
[6] Nguyen MP, Tan KH, Fung TC. Numerical models and parametric study on ultimate strength of CHS T-joints subjected to brace axial compression under fire condition. In: Tubular Structures XIII – Young, editor. The University of Hong Kong. 2010. p. 733.
[7] Meng J et al. Parametric analysis of mechanical behaviour of steel planar tubular truss under fire. J Constr Steel Res 2011;2010(67):75–83.
[8] Liu ML, Zhao JC, Jin M. An experimental study of the mechanical behavior of steel planar tubular trusses in a fire. J Constr Steel Res 2010;66(4):504–11.
[9] Chen C, Zhang W. Structural behaviors of steel roof truss exposed to pool fire. J Central South Univ 2012;19(7):2054–60.
[10] Yu W et al. Experimental study on mechanical behavior of an impacted steel tubular T-joint in fire. J Constr Steel Res 2011;67(9):1376–85.
[11] Jin M et al. Experimental and parametric study on the post-fire behavior of tubular T-joint. J Constr Steel Res 2012;70:93–100.
[12] Cheng C, Yongbo S, Jie Y. Experimental and numerical study on fire resistance of circular tubular T-joints. J Constr Steel Res 2013;85:24–39.
[13] He S-B et al. Experimental study on circular hollow section (CHS) tubular K-joints at elevated temperature. Eng Failure Anal 2013;34:204–16.
[14] Ozyurt E, Wang Y, Tan K. Elevated temperature resistance of welded tubular joints under axial load in the brace member. Eng Struct 2014;59:574–86.
[15] BSI, BS 5950: Part8: Code of Practice for the Fire Protection of Structural Steelwork, UK, 2003.
[16] Edwards M. Fire performance of SHS lattice girders. Tubular Structures V 2004;5:95.
[17] Boresi AP, Schmidt RJ. Advanced mechanics of materials. In: 6th Ed. ed. 2003: John Wiley and Sons.
[18] Cofer WF, Jubran JS. Analysis of welded tubular connections using continuum damage mechanics. J Struct Eng 1992;118(3):828–45.
[19] CEN, Design of Steel Structures. In: EN 1993-1-1-General Rules and Rules for Building, Part: editor. London: British Standard Institute; 2005.
[20] BSI, BS 476: Part 10: Guide to the principles, selection, role and application of fire testing and their outputs. UK, 2009.